SIXTH EUROPEAN ROTORCRAFT AND POWERED LIFT AIRCRAFT FORUM

Paper No. 15

A GALERKIN TYPE FINITE ELEMENT METHOD FOR ROTARY-WING AEROELASTICITY IN HOVER AND FORWARD FLIGHT

F.K. Straub and P.P. Friedmann
Mechanics and Structures Department
University of California at Los Angeles
Los Angeles, California, 90024, U.S.A.

September 16-19, 1980
Bristol, England

THE UNIVERSITY, BRISTOL, BS8 1HR, ENGLAND

A GALERKIN TYPE FINITE ELEMENT METHOD FOR ROTARY-WING AEROELASTICITY IN HOVER AND FORWARD FLIGHT[/]

F.K. Straub* and P.P. Friedmann

Mechanics and Structures Department
University of California at Los Angeles
Los Angeles, California, 90024, U.S.A.

ABSTRACT

A Galerkin finite element method for the spatial discretization of the nonlinear, nonselfadjoint, partial differential equations governing rotary-wing aeroelasticity is presented. This method reduces algebraic manipulative labor significantly when compared to the global Galerkin method based on assumed modes. Furthermore, the Galerkin finite element method is ideally suited to treat rotor blades with discontinuous mass and stiffness distribution and structurally redundant configurations as they appear in bearingless rotors. Implementation of the method is illustrated for the coupled flap-lag aeroelastic problem of hingeless rotor blades in hover and forward flight. Numerical results for stability and response illustrate the numerical properties and convergence behavior of the method. It is concluded that the Galerkin finite element method is a practical tool for solving rotary-wing aeroelastic stability and response problems.

1. Introduction

Increasing demands on helicopter performance and improved reliability and maintainability have led to the development of hingeless rotor systems and more recently to bearingless rotors. These systems are characterized by the elimination of flap and lag hinges and, for the bearingless rotor, the replacement of the pitch change bearing through an elastically twisted member which is commonly denoted as the flexbeam. Such rotor systems are designed by utilizing composites for the blade and flexbeam construction. A considerable amount of research has been directed toward the aeroelastic analysis of these rotors,[1] both for isolated blade[2-7] and coupled rotor fuselage models.[8-11]

Depending on the complexity of the analysis, the elastic properties of the blade have been modeled with a varying degree of sophistication. Most isolated blade analyses in forward flight and coupled rotor fuselage analyses rely on equivalent-hinge, spring-restrained, rigid blade models.[3,4,8,9] When elastic blade deformations are included, the dynamic equations of motion appear in partial differential form. Typically, Galerkin's method, based on

---

*Presently, Dynamics Engineer, Hughes Helicopters, Culver City, California

[/]This research was supported by the Structures Laboratory AVRADCOM Research and Technology Laboratories and NASA Langley Research Center, Hampton, Virginia, under NASA Grant NSG-1578.

mode shapes of the rotating blade, which are generated from the exact modes of a nonrotating, uniform beam, is used to eliminate the spatial dependence[1,2,5,6].

To fully understand the restrictions associated with this approach, the following aspects of rotary-wing aeroelasticity have to be kept in mind. The blade equations should be based on moderate deflection theory which leads to geometric nonlinearities in the structural, inertia and aerodynamic operators. Forward flight effects introduce periodic coefficients into the equations. Thus, to obtain actual aeroelastic stability boundaries, the equations are linearized about an appropriate equilibrium position and stability information is extracted from the eigendata associated with the linearized system. In forward flight the equilibrium position is periodic in time and depends on the trim state. Stability information is obtained through Floquet theory.

From the inspection of typical studies[2,6] it is clear that methods of solution based upon the modal Galerkin method lead to extremely cumbersome algebraic manipulations which have to be carried out manually or by alternative means such as algebraic manipulative systems. This complexity increases even further when more than one mode for each elastic degree of freedom is included in the analysis. Furthermore, the discontinuous mass and stiffness distribution and redundant construction of bearingless rotors[7] is not amenable to modeling by the Galerkin modal method as described above. One either has to resort to matrix methods[7,10] or use of mode shapes obtained through a finite element analysis.[11]

Recognizing the need for a discretization tool which overcomes the limitations of the modal Galerkin method, an extensive study was conducted[12] to develop a local Galerkin method,[13-15] leading to a finite element formulation of the rotary-wing aeroelastic problem. This method enables one to discretize the partial differential equations of motion directly, and consequently, a significant reduction in the algebraic manipulative labor required for the solution of the problem is accomplished. Furthermore, this Galerkin finite element method allows a unified treatment of structural and inertia, as well as aerodynamic terms. A normal mode coordinate transformation reduces the number of finite element nodal degrees of freedom considerably, however, without placing any restrictions on the number of modal coordinates retained. Lastly, this method is ideally suited for the incorporation of flexbeam dynamics into the aeroelastic analysis and the treatment of point masses and springs.

The general formulation of this Galerkin finite element method and its application to flap-lag dynamics of hingeless rotor blades in hover have been published previously.[16] The present paper concentrates on the following objectives: 1) The finite element formulation of the rotary-wing aeroelastic problem is extended to the flap-lag-torsion case in forward flight; 2) A newly developed quasilinearization technique,[17] for calculating the nonlinear periodic response, about which the equations are linearized, is shown to be compatible with the finite element formulation. Furthermore, within the context of the flap-lag problem in forward flight, the convergence of the method is established by numerical experimentation; and 3) The numerical properties and convergence behavior of the Galerkin finite element method are illustrated by applying it to the coupled flap-lag aeroelastic stability and response problem of hingeless blades in forward flight.

2. Equations of Motion

The blade equations of motion for the flap-lag torsion problem in forward flight are coupled nonlinear, nonconservative, partial differential equations with periodic coefficients. The structural operator[18] and the inertia and aerodynamic loads[6] have been derived previously. Therefore, only some of the basic assumptions underlying the derivation and the final form of the equations of motion and corresponding boundary conditions will be presented here, in as much as they are needed to illustrate the implementation of the Galerkin finite element method. Additional details can be found in Reference 12.

The geometry of the problem is described in Figures 1a and 1b. The basic assumptions in the derivation pertaining to hover have been presented in Reference 16; additional assumptions introduced in the present derivation are:

1) The helicopter is in straight, steady flight at constant speed ($\dot{\mu} = 0$). Rotor shaft dynamics are not considered ($\dot{\Omega} = 0$).

2) Root torsional deformation due to pitch link or control system flexibility occurs about the feathering axis.

3) The aerodynamic center, center of gravity and elastic center are distinct points. The tension center coincides with the elastic center ($x_{II} = 0$). The undeformed elastic axis is assumed to be a straight line and coincident with the feathering axis.

4) The blade is pretwisted, $\theta_B(\bar{x}_0)$, about the undeformed elastic axis.

5) The elastic torsional deformations occur about the deformed elastic axis.

6) Cross-sectional stiffness and inertia properties, offsets, and airfoil chord vary along the blade.

7) Structural or mechanical damping of viscous type is included.

8) Reversed flow is modeled in an exact manner.

9) Aerodynamic effects associated with forward flight introduce cyclic pitch variations; thus, the total geometric pitch angle is given by

$$\theta_G(\bar{x}_0,\psi) = \theta_B(\bar{x}_0) + \theta_0 + \theta_{1s} \sin\psi + \theta_{1c} \cos\psi \quad . \tag{1}$$

10) The inflow is represented by the following general functional form

$$\lambda(\bar{x},\psi) = \lambda_0 k_1(\bar{x}) + \lambda_s k_2(\bar{x}) \sin\psi + \lambda_c k_3(\bar{x}) \cos\psi \quad . \tag{2}$$

It should be pointed out that the influence of axial forces on the torsional rigidity of the rotor blade and the effect of cross-sectional warping due to torsion was neglected in Reference 18. The proper terms for this effect have recently become available.[19,20] Furthermore, the effects of stall and compressibility are not included in the aerodynamic loads of Reference 6. Although the above effects may be important for certain blades and certain flight conditions, no attempt was made to include them in the present study, since its primary objective is the application of the Galerkin finite element method.

Using the above assumptions, the coupled equations of motion for forward flight become[12]

Axial equilibrium:

$$\bar{T}_{,x} + p_{xI} = 0 \quad . \tag{3}$$

Lag equilibrium:

$$-(M_{3,x} + \bar{G}\bar{J}\,\phi_{,x}\,\bar{w}_{,xx} - \bar{v}_{,x}\,\bar{T})_{,x} - q_{3I,x} + p_{yI} + p_{yA} + p_{yD} = 0 \quad . \tag{4}$$

Flap equilibrium:

$$(M_{2,x} + \bar{G}\bar{J}\,\phi_{,x}\,\bar{v}_{,xx} + \bar{w}_{,x}\,\bar{T})_{,x} + q_{2I,x} + p_{zI} + p_{zA} + p_{zD} = 0 \quad . \tag{5}$$

Torsion equilibrium:

$$M_{x,x} + M_1 + q_{1I} + q_{xA} + q_{xD} = 0 \quad . \tag{6}$$

The corresponding boundary conditions at the free end, $\bar{x}_0 = 1$, are natural boundary conditions, expressing the fact that the shears, moments and tension at the blade tip are zero. At the cantilevered blade root, $\bar{x}_0 = 0$, the bending displacements and slopes (geometric quantities) are zero. The root torsional spring leads to a mixed boundary condition for torsion. Thus,

$$\text{at } \bar{x}_0 = 0: \qquad \bar{v} = \bar{w} = \bar{v}_{,x} = \bar{w}_{,x} = 0 \quad , \tag{7}$$

$$M_x - \bar{K}_\phi = 0 \quad . \tag{8}$$

$$\text{at } \bar{x}_0 = 1: \quad -M_{3,x} - \bar{G}\bar{J}\,\phi_{,x}\,\bar{w}_{,xx} + \bar{v}_{,x}\,\bar{T} - q_{3I,x} = 0 \quad , \tag{9}$$

$$M_{2,x} + \bar{G}\bar{J}\,\phi_{,x}\,\bar{v}_{,xx} + \bar{w}_{,x}\,\bar{T} - q_{2I,x} = 0 \quad , \tag{10}$$

$$M_3 = -M_2 = M_x = 0 \quad , \tag{11}$$

$$\bar{T} = 0 \quad . \tag{12}$$

Equations (3) - (12) are written in a general form which is most suitable when using the Galerkin finite element method to discretize the spatial dependence. Detailed expressions for the elastic moments (bending - M_1, M_2, M_3 and torsion - M_x) and the distributed loads (forces - p and moments - q, where inertia, aerodynamic and structural damping contributions are denoted by subscripts I, A, and D, respectively) are given in Reference 12. The tension $\bar{T}$ will be eliminated by using the axial equation (3) and corresponding boundary condition (12). The axial displacement, $\bar{u}$, will be replaced, using the commonly made assumption that the blade is inextensional in the axial direction. Thus, Equations (4) - (11) completely define the aeroelastic stability and response problem.

3. Application of the Galerkin Finite Element Method

The first step in solving the equations of motion, presented in the previous section, is the discretization of the spatial dependence. This is accomplished using a local Galerkin method of weighted residuals, resulting in a finite element formulation of the problem.

A detailed description of this Galerkin finite element method and its application to the flap-lag problem in hover have been presented in References 12 and 16. Therefore, only the major steps will be outlined here. However, special emphasis is placed on the appropriate modeling of the torsional degree of freedom.

First, an approximate global solution is substituted into the flap-lag-torsion equations of motion, Equations (4) - (6), and the corresponding boundary conditions. Recall, that in the extended Galerkin method the shape functions Φ_m need to satisfy only the geometric boundary conditions. Therefore, both the natural boundary conditions at the blade tip, Equations (9) - (11), and the mixed boundary condition, due to the root torsional spring, Equation (8), contribute to the boundary residual. The weighted Galerkin residual, obtained through appropriate combination of the weighted differential equation and boundary condition residuals is integrated by parts. After cancelling boundary terms, the problem is posed in the following integral form:

$$\int_0^1 \Bigg\langle [\Phi_m]^T_{,xx} \begin{Bmatrix} M_3 \\ -M_2 \\ 0 \end{Bmatrix}^g + [\Phi_m]^T_{,x} \begin{Bmatrix} -\bar{G}\bar{J}\,\phi_{,x}\,\bar{w}_{,xx} + \bar{v}_{,x}\,\bar{T} - q_{3I} \\ \bar{G}\bar{J}\,\phi_{,x}\,\bar{v}_{,xx} + \bar{w}_{,x}\,\bar{T} + q_{2I} \\ M_x \end{Bmatrix}^g$$

$$- [\Phi_m]^T \begin{Bmatrix} p_{yI} + p_{yA} + p_{yD} \\ p_{zI} + p_{zA} + p_{zD} \\ M_1 + q_{1I} + q_{xA} + q_{xD} \end{Bmatrix}^g \Bigg\rangle d\bar{x}_0 + [\Phi_{m(0)}]^T \begin{Bmatrix} 0 \\ 0 \\ \bar{K}_\phi \cdot \phi \end{Bmatrix}^g_{\bar{x}_0 = 0} = 0 \, . \tag{13}$$

Second, the global domain is divided into a number of subdomains or elements. In the interior of each element the displacements are assumed to be of the form

$$\{q^e\} = \begin{Bmatrix} \bar{v}^e \\ \bar{w}^e \\ \phi^e \end{Bmatrix} = \begin{bmatrix} \underset{\sim}{\gamma}^T & \underset{\sim}{0} & \underset{\sim}{0} \\ \underset{\sim}{0} & \underset{\sim}{\eta}^T & \underset{\sim}{0} \\ \underset{\sim}{0} & \underset{\sim}{0} & \underset{\sim}{\phi}^T \end{bmatrix} \begin{Bmatrix} \underset{\sim}{h}^e \\ \underset{\sim}{g}^e \\ \underset{\sim}{f}^e \end{Bmatrix}$$

$$= [\Psi(\bar{x}_e)] \{a^e(\psi)\} \quad . \tag{14}$$

For bending, the same cubic Hermite interpolation polynomials as in the hover case are used, see Appendix B. The nodal parameters are the lag and flap displacements and slopes at the element boundaries, see Figure 1b. This element satisfies the requirement of C_1 continuity of the global solution, since it provides interelement continuity for bending displacements and slopes. Bending strains vary linearly within the element which goes beyond the minimum requirement of constant strain within the element.

The torsion equation of motion is of second order with respect to the spatial variable. Thus, a linear interpolation will achieve the required C_0 continuity and constant strain. However, in the coupled bending-torsion analysis, it is desirable to use a torsion element which provides the same accuracy as the bending element. This allows discretization of the torsional variable with the same number of elements as needed for the adequate modeling of bending. In the present analysis, an improved torsion element, providing linear variation of torsional strain, is obtained by using the torsion deformation at the element mid-point as additional nodal parameter. Thus, $N = 3$, and the ϕ_n are quadratic interpolation polynomials,[21] given in Appendix B.

Figure 2 shows the relative accuracy of the finite element solution, as compared to the exact solution, for the first three bending and torsion frequencies of a nonrotating uniform beam. It is apparent that the cubic interpolation bending element and the quadratic interpolation torsion element provide approximately the same accuracy. The performance of the linear interpolation torsion element is considerably inferior. All elements exhibit uniform convergence, which had to be expected, since the finite element model for this conservative problem can be derived from a variational principle.

In general, refined finite elements can be obtained using any number of internal nodes. An alternative approach is the use of higher-order derivatives (second for bending and first for torsion, or higher) as nodal parameters. These higher-order elements, however, experience difficulties in modeling concentrated loads. Furthermore, the boundary conditions involving the higher-order derivatives must be satisfied. Therefore, such

elements were not considered.

In conclusion, it can be stated that the elements selected in the present study are the most basic (or simple) elements which yield a consistent formulation for coupled bending and torsion. This takes on an additional significance in light of the large number of nonlinear terms which have to be modeled. The exact form of the element interpolation polynomials $\underset{\sim}{\gamma}$, $\underset{\sim}{\eta}$, and $\underset{\sim}{\phi}$ is given in Appendix B.

The element displacements, Equation (14), are now extended over the global domain, by defining them as zero outside the particular element with which they are associated. Substituting the element displacements into the integrated Galerkin residual, given by Equation (13), yields the nonlinear, periodic element equations.

$$
\begin{aligned}
&([I_1^e] + [I_2^e(\underset{\sim}{a}^e)]\ \{\ddot{a}^e\} \\
&+ \Big([C_1^e] + [D_S^e] + [D_1^e] + [C_2^e(\underset{\sim}{a}^e)] + [T_2^e(\underset{\sim}{a}^e)] - [C_{Ax}^e(\underset{\sim}{a}^e)] + [C_{21}^e(\dot{\underset{\sim}{a}}^e)] \\
&\qquad + [D_{22}^e(\dot{\underset{\sim}{a}}^e)] + [D_{32}^e(\underset{\sim}{a}^e, \dot{\underset{\sim}{a}}^e)] + [D_2^e(\underset{\sim}{a}^e)] + [D_3^e(\underset{\sim}{a}^e)]\Big)\{\dot{\underset{\sim}{a}}^e\} \\
&+ \Big(\sum_{i=e+1}^{E} [T_2^{ei}(\underset{\sim}{a}^e)] - \sum_{i=1}^{e-1} [C_{Ax}^{ei}(\underset{\sim}{a}^i)]\Big)\{\dot{a}^i\} \\
&+ \Big([B_1^e] + [T_1^e] + [K_1^e] + [A_1^e] + [B_2^e(\underset{\sim}{a}^e)] + [K_2^e(\underset{\sim}{a}^e)] + [A_2^e(\underset{\sim}{a}^e)] + [A_3^e(\underset{\sim}{a}^e)]\Big) \\
&\cdot \{a^e\} + \{F_I^e\} + \{F_A^e\} + [B_c^1]\{a^1\}\,\delta_{e1} = \underset{\sim}{0} \quad \text{for} \quad e = 1,2,\ldots,E \ . \qquad (15)
\end{aligned}
$$

Detailed expressions for all element matrices in Equation (15), indicated by the superscript e, are defined in Reference 12. The structural operator is associated with the matrices $[B_1^e]$ and $[B_2^e]$. The axial tension results in the contributions represented by $[T_1^e]$, $[T_2^e]$ and $[T_2^{ei}]$. The inertia loads are included in $[I_1^e]$, $[I_2^e]$, $[C_1^e]$, $[C_2^e]$, $[K_1^e]$, $[K_2^e]$, $\{F_I^e\}$, $[C_{Ax}^e]$ and $[C_{Ax}^{ei}]$, where the last two matrices are due to the axial shortening effect. The aerodynamic loads are contained in the $[D_1^e]$, $[D_2^e]$, $[D_{22}^e]$, $[D_3^e]$, $[D_{32}^e]$, $[A_1^e]$, $[A_2^e]$, $[A_3^e]$ and $\{F_A^e\}$ matrices. The structural damping effect is represented by $[D_S^e]$. Finally, the $[B_c^1]$ matrix accounts for the root torsional condition, where the Kronecker delta, δ_{e1}, indicates that

this term is only present in the first element, i.e., the element at the root of the blade.

The functional dependence of the element matrices on the nodal displacements is as indicated in Equation (15). Note, that the matrices in Equation (15) have both single and double numerical subscripts. The first subscript is an identifier of nonlinear terms. A first subscript having a value of 2 or 3 is indicative of quadratic or cubic terms, respectively. A second subscript is attached to all velocity-dependent element matrices. All element matrices are evaluated using six-point Gaussian quadrature. The nonuniform element properties are included in the numerical integration.

Next, the element matrices are assembled into the complete system matrices. The nodal parameters within the nonlinear element matrices are replaced by their modal representation,

$$\{a\} = [\Lambda]\{q\} \quad , \tag{16}$$

using M_L lag, M_F flap, and M_T torsion free vibration mode shapes of the rotating blade which are computed using the finite element method. Subsequently, the modal reduction process is completed by pre- and post-multiplying the system matrices with the modal transformation matrix, $[\Lambda]$, and its transpose. For more details regarding the treatment of nonlinear terms, see Reference 12.

The final equations of motion, in terms of the reduced set of M modal degrees of freedom, can be written symbolically as:

$$\underset{\sim}{G} = [m(\underset{\sim}{q})]\{\ddot{q}\} + [d(\underset{\sim}{q}, \underset{\sim}{\dot{q}})]\{\dot{q}\} + [k(\underset{\sim}{q})]\{q\} + \{f\} = \underset{\sim}{0} \quad . \tag{17}$$

All matrices in Equation (17) are defined in Reference 12. Note, that the inertia, damping, and stiffness terms have both linear and nonlinear contributions. Also recall, that for forward flight, most matrices have periodic coefficients, i.e.,

$$\underset{\sim}{G}(q, \dot{q}, \ddot{q}, \psi) = \underset{\sim}{G}(q, \dot{q}, \ddot{q}, \psi + 2\pi) \quad ,$$

with the common period being 2π, which corresponds to one blade revolution.

4. Method of Solution

In forward flight the aeroelastic stability and response of isolated rotor blades is strongly coupled with the overall equilibrium of the helicopter.[1,3,5] The trim state of the helicopter, obtained using either the propulsive or moment trim procedures developed in Reference 17, is used as input to the aeroelastic analysis of the blade.

A solution to Equation (17) must provide both stability and response information. Finite element solutions to nonlinear dynamic problems are mainly restricted to finding the transient response under impulse loading. Instead of relying on a direct numerical integration, with its known drawbacks for equations with periodic coefficients, in the present study the aeroelastic stability of the blade is obtained explicitly from eigendata extracted from the linearized system. The approximate nonlinear steady-state response of the blade is used as equilibrium position about which the perturbation equations are linearized. This nonlinear, time dependent equilibrium position is evaluated by iterative application of a method developed to obtain the steady-state response of linear periodic systems.[17] A brief description of this procedure, emphasizing the finite element formulation of the problem follows.

First, the finite element equations (17) are expanded in a Taylor series about a previous solution, keeping only linear terms. During the k-th iteration step, the previous solution is denoted by q^{k-1}. This solution must be periodic in ψ and its derivatives $\dot{q}^{k-1}$, $\ddot{q}^{k-1}$ are known. The linearized equations now take the form:

$$[M^k]\{\ddot{q}^k\} + [C^k]\{\dot{q}^k\} + [S^k]\{q^k\} - [C^k]\{\dot{q}^{k-1}\} - [S^k]\{q^{k-1}\} + \{F^k\} = 0 \quad , \tag{18}$$

where

$$[M^k] = \frac{\partial G}{\partial \ddot{q}}(q^{k-1}) \quad , \tag{19a}$$

$$[C^k] = \frac{\partial G}{\partial \dot{q}}(q^{k-1}, \dot{q}^{k-1}) \quad , \tag{19b}$$

$$[S^k] = \frac{\partial G}{\partial q}(q^{k-1}, \dot{q}^{k-1}, \ddot{q}^{k-1}) \quad , \tag{19c}$$

$$[F^k] = [d(q^{k-1}, \dot{q}^{k-1})]\{\dot{q}^{k-1}\} + [k(q^{k-1})]\{q^{k-1}\} + [f] \quad . \tag{19d}$$

Details on the evaluation of the derivatives of G can be found in Reference 12. For convenient numerical treatment, Equation (18) is transformed into first-order state variable form.

$$\{\dot{y}^k\} = \begin{Bmatrix} \dot{\underset{\sim}{q}}^k \\ \\ \dot{\underset{\sim}{q}}^k \end{Bmatrix}$$

$$= [A^k(\underset{\sim}{y}^{k-1}, \dot{\underset{\sim}{y}}^{k-1}, \psi)]\{y^k\} + \{b^k(\underset{\sim}{y}^{k-1}, \psi)\} \qquad (20)$$

where

$$[A^k] = \begin{bmatrix} -[M^k]^{-1}[C^k] & \vert & -[M^k]^{-1}[S^k] \\ & \vert & \\ [I] & \vert & [0] \end{bmatrix} , \qquad (21)$$

$$\{b^k\} = \begin{Bmatrix} [M^k]^{-1}([C^k]\{\dot{q}^{k-1}\} + [S^k]\{q^{k-1}\} - \{F^k\} \\ \\ \{0\} \end{Bmatrix} . \qquad (22)$$

Both $[A^k]$ and $\{b^k\}$ are periodic in ψ (with period 2π) and depend on the previous solution $\underset{\sim}{y}^{k-1}$.

The solution of the linearized Equation (20), i.e., the k-th iterative periodic response $\underset{\sim}{y}^k(\psi)$, is calculated by determining the initial conditions $\underset{\sim}{y}^k(0)$ required for time-history integration, to yield a periodic response.[22] Numerical integration of Equation (20) using $\underset{\sim}{y}^k(0)$ yields $\underset{\sim}{y}^k(\psi)$. The periodicity of the response is checked by integrating over several periods (i.e., blade revolutions) until the Fourier coefficients of the response obtained in two subsequent periods agree within a desired accuracy.

This periodic response, $\underset{\sim}{y}^k$, is then used as a previous solution for the next iteration step. This process is continued until convergence is achieved, at which step $\underset{\sim}{y}^k$ represents the periodic steady-state response of the nonlinear system, which is denoted as $\bar{\underset{\sim}{y}}$. This solution is then used as the equilibrium position for the stability calculations.

In the present study, two options for initiating the quasilinearization process were implemented. Stability information in forward flight is usually plotted as a function of the advance ratio μ. Therefore, at a given value of μ, either the linear response of the system (with all nonlinear terms deleted), or the nonlinear response for a previous lower value of μ was used as initial solution.

Stability was studied by deriving linearized perturbation equations about the known equilibrium position $\bar{\underset{\sim}{y}}(\psi)$. This leads to a linear,

homogeneous periodic system.

$$\{\Delta\dot{y}\} = [A(\bar{y}, \dot{\bar{y}}, \Psi)]\{\Delta y\} \quad , \tag{23}$$

where [A] is defined by Equation (21) with y^{k-1} replaced by $\bar{y}$. According to Floquet theory, the characteristic exponents, $\lambda_k = \zeta_k + i\omega_k$, of the associated transition matrix at the end of one period, $[\Phi(2\pi)]$, are indicative of stability.[1,5] The linearized system, Equation (23), is stable when $\zeta_k < 0$ for all k.

At this point it should be pointed out that for each time step in the numerical integration of Equation (20) and in the calculation of the transition matrix, the finite element discretization process, i.e., formulation of Equations (15), (17), (18) and (20) has to be repeated. Efficient programming and use of efficient methods to calculate stability and response[17,23] is, therefore, crucial for the effective treatment of this problem.

5. Results and Discussion

Results in the present paper illustrate the application of the Galerkin finite element method to rotary-wing aeroelastic problems in forward flight. The bending free vibration problem of a cantilever rotating beam and the coupled flap-lag aeroelastic stability of hingeless rotor blades in hover were considered in Reference 16. Figure 3 shows typical stability boundaries for flap-lag in hover. It also illustrates the excellent agreement obtained with the Galerkin finite element method and the modal Galerkin method. These and other results[16] showed the Galerkin finite element method to be a practical tool for formulating and solving rotary-wing aeroelastic problems. It was concluded that four or five elements are sufficient to model the bending dynamics in hover and that for certain configurations, stability is determined by the second lag mode.

5.1 Assumptions and Data Used in Generating Results

Results for forward flight deal with the coupled flap-lag aeroelastic problem of hingeless rotors. In view of the novel features of the present research, where a finite element solution is given for the stability and response of nonlinear, nonconservative, periodic systems, torsional dynamics were excluded in the computer code.

Numerical results are presented in two groups. First, the numerical properties of the solution procedure for the discretized dynamic equations, outlined in Section 4, are investigated. These results, presented in Figures 4 - 9, are based on propulsive trim[5] with a weight coefficient of $C_W = 0.01$ and the following data:

$$\bar{\omega}_{L1} = 1.417; \quad \bar{\omega}_{F1} = 1.087; \quad \bar{b} = 0.0313; \quad \gamma = 5.0;$$

$$\sigma = 0.05 \; ; \quad E = 3 \quad ; \quad M = 2 \quad ; \quad R_c = 1.0.$$

The second group of results, presented in Figures 10 - 18, deals with

the convergence properties of the Galerkin finite element method. Response plots show the converged nonlinear steady-state response which is subsequently used in the linearized stability analysis. Trim values are calculated using the improved propulsive trim procedure of Reference 17, with $C_W = 0.05$ (0.01) and the fuselage pitching moment and the various trim offsets set to zero. The configuration parameters, chosen so that the soft in-plane blade has properties somewhat similar to those of the Boelkow BO-105 rotor,[24] are:

$$\bar{\omega}_{Ll} = 0.732 \ (1.417); \ \bar{\omega}_{Fl} = 1.125; \ \bar{b} = 0.0275; \ n_b = 4 \ ;$$

$$\gamma = 5.5; \ \sigma = 0.07; \ N_{psi} = N_{rki} = 60; \qquad N_h = 10.$$

Parameters which remained unchanged for all forward flight results are:

$$\rho_A = 1.23 \ kg/m^3 \ (0.00238 \ slugs/ft^3); \ a = 2\pi; \ C_{dO} = C_{DP} = 0.01;$$

$$x_L = 0.0; \ x_U = 1.0; \ \bar{e}_1 = \beta_p = \bar{x}_A = \gamma_F = 0.0; \ \eta_{SL} = \eta_{SF} = 0.0 \ .$$

Furthermore, blade pretwist was set to zero and the blade properties were assumed to be uniform over the span. The inflow was modeled to be uniform, i.e.,

$$\lambda = \lambda_0 = \mu \tan \alpha_R + \frac{C_T}{2\sqrt{\mu^2 + \lambda_0^2}} \ .$$

5.2 Results

The first group of results, presented in Figures 4 through 9, is intended to illustrate the effect of the numerical parameters associated with the quasilinearization technique[17] outlined in Section 4. Figures 4 and 5 show the effect of the number of harmonics, N_h, used in the Fourier series representation of the periodic blade response.[12] The blade tip displacements, normalized with respect to the length of the elastic portion of the blade, are plotted. While the lag response, Figure 4, changes only a little when using ten as compared to one harmonic, a noticeable change can be seen for the flap response in Figure 5. This is also reflected in the stability results[12], in as much as the flap damping changes remarkably with the number of harmonics, whereas the lag damping remains basically unchanged. Inspection of the Fourier coefficients of the response plotted in Figures 4 and 5 showed that while it is essential to retain more than the first harmonics, it probably would be sufficient to use the first four harmonics. These results clearly illustrate that analyses using the harmonic balance

technique with only the first harmonics to calculate the time-dependent equilibrium position[5,6] can lead to inaccurate predictions of system damping. In all subsequent calculations, ten harmonics ($N_h = 10$) were used.

Figures 6 through 8 illustrate the effect of nonlinear terms on system steady-state response and stability. Response results are shown with the number of quasilinearization steps, k, as parameter. The lag response, Figure 6, and more so the flap response, Figure 7, change noticeably when going from the linear solution (all nonlinear terms neglected), $k = 0$, to the linearized solution, $k = 1$. When performing an additional iteration step, i.e., considering an approximation to the fully nonlinear solution, $k = 2$, the response remains practically unchanged. This implies that the linearized response is a sufficiently accurate representation of the converged nonlinear response.

Figure 8 shows the convergence of the real part of the characteristic exponents, a measure of stability, with the number of quasilinearization steps. A decrease in percentage error value corresponds to a decrease in stability margin. Analysis of the linear system ($k = 0$, i.e., all nonlinear terms neglected) will generally lead to large errors in the predicted damping values. In particular, this holds for the lag degree of freedom which is affected considerably by nonlinear aeroelastic coupling terms. At intermediate advance ratios, $\mu = 0.2$, one iteration step ($k = 1$, i.e., linearization about the linear equilibrium position) is sufficient. At high advance ratios, $\mu = 0.4$, a second iteration step ($k = 2$, i.e., linearization about the linearized equilibrium position) might be required to predict system stability. The larger error, at $k = 1$, for the flap degree of freedom, as compared with lag, can be directly related to the effect of nonlinear terms on the flap response as shown in Figure 7. It should be pointed out, however, that the influence of nonlinearities in this particular case is somewhat exaggerated due to the high value of the weight coefficient ($C_W = 0.01$).

In Figure 9 the effect of the number of azimuthal steps on system stability is shown. In all cases the same number of steps (per revolution) was used to calculate the initial conditions and stability, N_{psi}, and to determine the response by numerical integration, N_{rki}. The relative change of the real part of the characteristic exponents at $\mu = 0.4$ is plotted. The solution, with 120 steps, was used as reference. Note that the flap degree of freedom does not have complex conjugate exponents, i.e., two distinct real parts are associated with it. Overall, results based on forty steps are in excellent agreement. (The same was concluded for response, although the results are not shown.) Even twenty steps give only one percent error. In all subsequent calculations, sixty steps ($N_{psi} = N_{rki} = 60$), were used. Another interesting aspect of Figure 9 is that the flap results converge slower than the lag results. This confirms the previous conclusion that higher harmonic contributions are more significant for the flap degree of freedom.

Additional results[12], not presented here, showed that the initial conditions in Equation (23) do indeed lead to excellent periodicity of the response. Plots of the blade tip deflections during the first ($N_{rev} = 1$) and second ($N_{rev} = 2$) blade revolution showed very little difference. The response during the second and third blade revolution could not be distinguished on the plots. This indicates that the effect of approximations and numerical errors in the actual calculation of the initial conditions

(which theoretically insure a periodic response) is usually corrected with the integration over the second blade revolution.

From the numerical experience gained in this study, represented by Figures 4 - 9, it was concluded that a maximum change of each Fourier coefficient of less than 10^{-3} is sufficient to indicate periodicity and convergence of the nonlinear response. Recall, that in the derivation of the equations of motion, the displacements were assumed to be of order $\varepsilon_D \approx 0.2$ and terms of $O(\varepsilon_D^2)$ were neglected, as compared to terms of $O(1)$. Therefore, this error control quantity is also logically consistent with the ordering scheme. All results were obtained by using the linear equilibrium position as the initial guess in the quasilinearization procedure. A test case showed no gains in accuracy or computing times when using the converged nonlinear response from a previous lower value of μ as the initial guess.

Lastly, it should be pointed out that the results presented so far were for a relatively high loading ($C_W = 0.01$). The choice of parameters made above should thus be considered conservative when cases with a more realistic blade loading are considered and, therefore, should also be adequate when more elements and mode shapes are used in the analysis.

The convergence properties of the Galerkin finite element method are considered next by changing the number of elements used or the number of mode shapes retained in the normal mode transformation. Aeroelastic stability is studied by plotting the real part of the characteristic exponent, ζ_k, versus the advance ratio μ. The system is stable if all $\zeta_k < 0$. All these results are based on the second set of configuration parameters. The relative change in the real part of the characteristic exponent versus the number of elements is shown in Figure 10 for the soft in-plane blade, $\bar{\omega}_{L1} = 0.732$, and elastic coupling $R_c = 0.6$. The number of modes was kept constant at two. As reference, the five-element solution was used. It is apparent that excellent convergence is achieved, in particular, when considering that the results in Figure 10 are for a high advance ratio, $\mu = 0.4$. Interestingly, the accuracy for the flap degree of freedom is much higher than that for lag. This can be attributed to the lower stability margin for lag; see Figures 11 and 12. Overall, the three-element solution can be considered sufficiently accurate. It should be kept in mind, however, that the configuration in Figure 10 is stable. For a more critical case, more elements might be required to model the system accurately. Finally, it is interesting to compare Figure 10 with the accuracy for the first bending frequency of a nonrotating beam in Figure 2. As expected, the solution of the aeroelastic problem does require a larger number of elements than the free vibration problem. In addition, it can be seen that convergence is uniform in this case but not one sided, as indicated by $(-\%)$ for the lag degree of freedom.

Figures 11 and 12 show system stability when changing the number of modes from two to four, while keeping the number of elements constant at $E = 4$. The aeroelastic damping for the fundamental modes, ζ_{1L} and ζ_{1F}, remains unchanged when using four modes as compared to two modes. The damping, i.e., real part of the characteristic exponents, for both predominant flap modes is practically constant for all advance ratios. The absolute value of ζ_{2F} is somewhat lower than that for the first flap mode, ζ_{1F}, however, both modes are strongly damped. The first lag mode has its lowest damping values at moderate advance ratios, $\mu = 0.1 - 0.2$. When the

advance ratio is increased, the results indicate that the forward flight aerodynamics have a stabilizing effect. Overall, the smallest stability margin occurs at hover, $\mu = 0.0$, for the second predominant lag mode. However, with increasing advance ratios, more aerodynamic damping is fed into the second lag mode. For advance ratios, $\mu > 0.2$, the real parts of the characteristic exponents for both lag modes, ζ_{1L} and ζ_{2L}, are roughly the same.

The effect of the number of modes retained in the modal reduction process on the blade response at $\mu = 0.4$ is illustrated in Figures 13 and 14. The response of the second lag mode, h_2, is very small. Only in the reversed flow region can it be distinguished from zero. The second flap mode response, g_2, is more significant. The behavior of the response associated with the first lag and flap mode, respectively, varies accordingly. For lag, the response of the first mode does not change significantly when going from two to four modes in the analysis. For flap, on the other hand, there is a sizeable change. When the response of the first and second flap mode (from the four-mode analysis, $M = 4$) are added together, its maximum value is roughly eight percent larger than that of the response based on the two-mode analysis $(M = 2)$.

The effect of the number of modes used in the analysis is further investigated by considering the stability of a stiff in-plane blade, $\bar{\omega}_{L1} = 1.417$, with elastic coupling $R_c = 0.8$, in propulsive trim $(C_W = 0.01)$. Results for the real part of the characteristic exponents are obtained by using two and four modes. In both cases, the blade is represented by four elements. The stability curves in Figures 15 and 16 exhibit the same general behavior as encountered for the soft in-plane blade (Figures 11 and 12). There are, however, two important differences. The second lag mode is unstable at $\mu = 0.0$, i.e., ζ_{2L} is positive. Thereafter, the forward flight aerodynamics introduce a considerable amount of damping, so that at $\mu = 0.1$ the second lag mode is more stable than the first lag mode by a factor of five. A further increase in the advance ratio changes the value of ζ_{1L} such that it approaches the value of ζ_{2L}, and at $\mu = 0.4$, they are practically the same. The other interesting point is that at $\mu = 0.4$ only the four-mode solution exhibits splitting of the characteristic exponents (real part) associated with the first flap mode. The two-mode solution does not capture this effect.

Results presented in Figures 11 - 16 indicate that for both response and stability it is important to retain four modes in the analysis. Recall, that in the hover case the second predominant lag mode itself was the cause for system instability at certain values of the lag frequency $\bar{\omega}_{L1}$; see Figure 3. In the forward flight case such an instability was not observed; however, the presence of the second lag and flap mode lowered the stability margin and affected the response of the flap degree of freedom. Although these changes did not result in a critical condition, they might have an effect on blade bending moments and shears.

The effect of the elastic coupling parameter, R_c, on the stability of the first and second predominant lag mode is shown in Figures 17 and 18, respectively, for the soft in-plane blade. The stability margin of the first lag mode (Figure 17) increases proportionally with the value of R_c throughout the entire range of advance ratios. The least stable configuration is obtained for zero elastic coupling, at low advance ratios $(\mu =$

0.1 - 0.2). The behavior of the second lag mode, (Figure 18), is quite different. The variation of damping versus the advance ratio depends strongly on the value of R_c. At low advance ratios, elastic coupling is destabilizing; above $\mu = 0.3$ it is stabilizing. Lastly, it should be mentioned that the predominant flap modes are very stable and the damping associated with them remained almost constant when the elastic coupling was changed. The same observation was made for the hover case.

Additional results obtained in the course of the present study[12] are not presented here due to the lack of space.

All flap-lag forward flight results were generated on an IBM 3033 computer. To find the converged, nonlinear, periodic response and linearized stability for one value of advance ratio, approximately 30 CPU seconds were needed in the three-element two-mode case. When using four elements, 40 CPU seconds were required. In the case of four elements and four modes, this value increased to approximately 100 CPU seconds. The computation of the aerodynamic element matrices takes up roughly 50 percent of these CPU times. In comparison, for the modal Galerkin method, solution of the flap-lag-torsion problem[17] (six modes) 100 CPU seconds were required.

6. Conclusions

This paper presents the extension of a previously formulated Galerkin-type finite element method for nonselfadjoint, nonlinear aeroelastic rotary-wing problems[16] to the forward flight case. From the numerical results presented for the flap-lag aeroelastic stability and response of hingeless helicopter rotor blades in hover[16] and in forward flight, the following conclusions are drawn.

1. The Galerkin finite element method is a practical tool for formulating and solving rotary-wing aeroelastic problems. Since spatial discretization is applied directly to the partial differential equations, algebraic manipulative labor is reduced significantly when compared to the application of the global Galerkin method to similar problems. However, more computer time is spent in calculations, in particular, when dealing with forward flight.

2. Four or five elements are sufficient to capture the bending dynamics of the blade in hover with the same accuracy as the global Galerkin method. For practical forward flight cases, three or four elements suffice.

3. Normal mode transformation, combined with the Galerkin finite element formulation, reduces the number of nodal degrees of freedom significantly and enables one to deal efficiently with complex problems. Complete freedom regarding the number of modes to be used is retained.

4. For the flap-lag problem in hover it is essential to use two modes for each elastic degree of freedom, since the second lag mode determines system stability for certain values of elastic coupling.

5. The flap-lag problem in forward flight is basically stable. The lowest stability margins are associated with the lag degree of freedom at moderate advance ratios. Inclusion of two modes for each elastic degree of freedom lowers the stability margin; it also affects the response.

6. For the flap-lag case, nonlinearities affect system stability only at high advance ratios. Comparison with coupled flap-lag-torsion results[17] shows that presence of torsion increases system sensitivity to nonlinear terms and changes predicted damping levels significantly. System response, based on the linearized and, in some cases, even linear equations seems to be sufficiently accurate.

7. Higher harmonic contributions to the periodic blade motion are significant, especially for flap stability and response.

8. Future applications of the Galerkin finite element method should include the torsional degree of freedom and concentrate on the modeling of bearingless flexbeam-type rotors.

REFERENCES

1. Friedmann, P., "Recent Developments in Rotary-Wing Aeroelasticity," Journal of Aircraft, Vol. 14, No. 11, November 1977, pp. 1027-1041.

2. Hodges, D.H., and Ormiston, R.A., "Stability of Elastic Bending and Torsion of Uniform Cantilever Rotor Blades in Hover with Variable Structural Coupling," NASA TND-8192, April 1976.

3. Peters, D.A., "Flap-Lag Stability of Helicopter Rotor Blades in Forward Flight," Journal of the American Helicopter Society, Vol. 20, No. 4, October 1975, pp. 2-13.

4. Schrage, D.F., and Peters, D.A., "Effect of Structural Coupling Parameters on the Flap-Lag Forced Response of a Rotor in Forward Flight Using Floquet Theory," Vertica - The International Journal of Rotorcraft and Powered Lift Aircraft, Vol. 3, No. 2, 1979, pp. 177-185.

5. Friedmann, P., and Shamie, J., "Aeroelastic Stability of Trimmed Helicopter Blades in Forward Flight," Vertica - The International Journal of Rotorcraft and Powered Lift Aircraft, Vol. 1, No. 3, 1977, pp. 189-211.

6. Shamie, J., and Friedmann, P., "Effect of Moderate Deflections on the Aeroelastic Stability of a Rotor Blade in Forward Flight," Paper No. 24, Proceedings of the Third European Rotorcraft and Powered Lift Aircraft Forum, Aix-en-Provence, France, September 1977.

7. Bielawa, R.L., "Aeroelastic Characteristics of Composite Bearingless Rotor Blades," Journal of the American Helicopter Society, Vol. 22, No. 4, October 1977, pp. 2-9, 19.

8. Huber, H.B., "Effect of Torsion Flap-Lag Coupling on Hingeless Rotor Stability," AHS Preprint No. 731, Proceedings of the 29-th Annual National Forum of the American Helicopter Society, Washington, D.C., 1973.

9. Ormiston, R.A., "Aeromechanical Stability of Soft Inplane Hingeless Rotor Helicopters," Paper No. 21, Proceedings of the Third European Rotorcraft and Powered Lift Aircraft Forum, Aix-en-Provence, France, September 1977.

10. Hodges, D.H., "An Aeromechanical Stability Analysis for Bearingless Rotor Helicopters," Journal of the American Helicopter Society, Vol. 24, No. 1, January 1979, pp. 1-9.

11. Lytwyn, R.T., "Aeroelastic Stability Analysis of Hingeless Rotor Helicopters in Forward Flight Using Blade and Airframe Normal Modes," AHS Preprint No. 80-24, Proceedings of the 36-th Annual Forum of the American Helicopter Society, Washington, D.C., 1980.

12. Straub, F.K., "Application of the Finite Element Method to Rotary-Wing Aeroelasticity," Ph.D. Dissertation, School of Engineering and Applied Science, University of California, Los Angeles, April 1980 (to be published as UCLA ENG-report).

13. Zienkiewicz, O.C., The Finite Element Method, McGraw-Hill, 3rd ed., 1977, pp. 42-92.

14. Kikuchi, F., "A Finite Element Method for Non-Self-Adjoint Problems," International Journal of Numerical Methods in Engineering, Vol. 6, 1973, pp. 39-54.

15. Hutton, S.G., and Anderson, D.L., "Finite Element Method: A Galerkin Approach," Journal of Engineering Mechanics Division of ASCE, October 1971, pp. 1503-1520.

16. Friedmann, P.P. and Straub, F., "Application of the Finite Element Method to Rotary-Wing Aeroelasticity," Journal of the American Helicopter Society, Vol. 25, No. 1, January 1980, pp. 36-44.

17. Friedmann, P.P., and Kottapalli, S.B.R., "Rotor Blade Aeroelastic Stability and Response in Forward Flight," Paper No. 14, Proceedings of the Sixth European Rotorcraft and Powered Lift Aircraft Forum, Bristol, England, September 1980; a more detailed version to appear as UCLA-ENG report).

18. Rosen, A., and Friedmann, P., "Nonlinear Equations of Equilibrium for Elastic Helicopter or Wind Turbine Blades Undergoing Moderate Deformations," School of Engineering and Applied Science Report, UCLA-ENG-7718, University of California, Los Angeles, January 1977 (revised June 1977); also available as NASA CR-159478, December 1978.

19. Rosen, A., "The Effect of Initial Twist on the Torsional Rigidity of Beams - Another Point of View," ASME - Journal of Applied Mechanics, Vol. 47, June 1980, pp. 389-392.

20. Hodges, D.H., "Torsion of Pretwisted Beams Due to Axial Loading," ASME - Journal of Applied Mechanics, Vol. 47, June 1980, pp. 393-397.

21. Bathe, K.-J., and Wilson, E.L., Numerical Methods in Finite Element Analysis, Prentice Hall, 1976, pp. 127-130.

22. Kottapalli, S.B.R., Friedmann, P.P., and Rosen, A., "Aeroelastic Stability and Response of Horizontal Axis Wind Turbine Blades," AIAA Journal, Vol. 17, No. 2, December 1979, pp. 1381-1389.

23. Friedmann, P., Hammond, C.E., and Woo, T., "Efficient Numerical Treatment of Periodic Systems with Application to Stability Problems," International Journal of Numerical Methods in Engineering, Vol. 11, 1977, pp. 1117-1136.

24. Staley, J.A., "Validation of Rotorcraft Flight Simulation Program Through Correlation with Flight Data for Soft-in-Plane Hingeless Rotors," USAAMRDL-TR-75-50, January 1976.

APPENDIX A: LIST OF SYMBOLS

a = two-dimensional lift curve slope

$\underset{\sim}{a}^e$ = element nodal displacement vector

$\underset{\sim}{a}$ = system nodal displacement vector

$[A], [A^k]$ = coefficient matrix of dynamic equations in first-order state variable form, Eqs. (21), (23)

$[A_1^e], [A_2^e] [A_3^e]$ = aerodynamic stiffness matrices

$\bar{b} = b/R$ = airfoil semichord

$\{b^k\}$ = forcing vector in the linearized dynamic equations in first-order state variable form, Eq. (22)

$[B_1^e], [B_2^e]$ = element stiffness matrices

$[B_c^1]$ = boundary condition term, due to root-torsional stiffness

C_{dO} = blade profile drag coefficient

C_{DP} = helicopter parasite drag coefficient

C_T = rotor thrust coefficient, $T/\rho_A \pi R^2 \Omega^2 R^2$

C_W = helicopter weight coefficient, $W/\rho_A \pi R^2 \Omega^2 R^2$

$[C^k]$ = damping matrix in linearized dynamic equations, Eq. (18)

$[C_{Ax}^e], [C_{Ax}^{ei}]$ = matrices due to axial shortening effect

$[C_1^e], [C_2^e], [C_{21}^e]$ = element matrices, velocity dependent inertia loads

$[d]$ = damping matrix in dynamic equations, Eq. (17)

$[D_1^e], [D_2^e], [D_3^e], [D_{22}^e], [D_{23}^e]$ = aerodynamic damping matrices

$[D_S^e]$ = structural damping element matrix

$\bar{e}_1 = e_1 / \ell$ = blade root offset from axis of rotation, Fig. 1

$\hat{e}_x, \hat{e}_y, \hat{e}_z$ = unit vector triad in x_0, y_0, and z_0 directions, respectively, before deformation, Fig. 1a

$\hat{e}'_x, \hat{e}'_y, \hat{e}'_z$ = unit vector triad $\hat{e}_x$, $\hat{e}_y$, and $\hat{e}_z$, respectively, after deformation, Fig. 1b

E = number of finite elements

$\underset{\sim}{f}^e$ = element torsion nodal displacements, Eq. (14)

$\{f\}$ = forcing vector in dynamic equations, Eq. (17)

$\{F_I^e\}, \{F_A^e\}$ = inertia and aerodynamic loads, respectively, independent of displacements

$\{F^k\}$ = operator, Eq. (18)

$\underset{\sim}{g}^e$ = element flap displacements, Eq. (14)

g_m = generalized coordinate, m-th flap mode

GJ = blade torsional rigidity, $\bar{GJ} = GJ/(m_o \Omega^2 \ell^4)$

$\underset{\sim}{G}$ = operator, Eq. (17)

$\underset{\sim}{h}^e$ = element lag displacements, Eq. (14)

h_m = generalized coordinate, m-th lag mode

I_b = blade mass moment of inertia in flap

$[I]$ = unit matrix

$[I_1^e], [I_2^e]$ = element matrices, acceleration dependent inertia loads

k = index, identifying the quasilinearization steps

k_1, k_2, k_3 = inflow functions, Eq. (2)

K_ϕ = root torsional spring stiffness, $\bar{K}_\phi = K_\phi/(m_o \Omega^2 \ell^3)$

$[k]$ = stiffness matrix in dynamic equations, Eq. (17)

$[K_1^e], [K_2^e]$ = element matrices, displacement dependent inertia loads

ℓ = length of elastic portion of blade, Fig. 1a

m_o = reference value for mass per unit length of blade

M = total number of modes used in analysis

M_L, M_F, M_T = number of lag, flap, and torsion modes, respectively, used in analysis

M_x, M_1, M_2, M_3 = elastic moments, nondimensional

$[m]$ = mass matrix, Eq. (17)

$[M^k]$ = mass matrix in linearized dynamic equations, Eq. (18)

n_b = number of blades in rotor

N = number of element shape functions for each elastic degree of freedom

N_h = number of harmonics used in the Fourier analysis of the periodic response

N_{psi} = number of steps per revolution when computing the transition matrices and initial conditions

N_{rki} = number of steps per revolution used in the Runge-Kutta integration

N_{rev} = index, identifying consecutive rotor revolutions

$\underline{p}$ = distributed external force vector per unit length of blade, nondimensional; subscripts I, A, and D represent inertia, aerodynamic and structural damping contributions, respectively

$\{q\}$ = vector of unknown lag, flap, and torsion displacements

$\{q^e\}$ = element, (local) approximation to $\{q\}$

$\{q\}$ = vector of generalized modal coordinates, Eq. (16)

$\underline{q}$ = distributed external moment vector per unit length of blade, nondimensional

R_c = blade elastic coupling parameter

R = blade radius, Fig. 1a

$[S^k]$ = stiffness matrix in linearized dynamic equations, Eq. (18)

$\bar{T}$ = tensile force in blade, nondimensionalized by $(m_o \Omega^2 \ell^2)$

$[T_2^e], [T_2^{ei}]$ = tension matrices

$\bar{u} = u/\ell$ = axial displacement of blade, inextensional

$\bar{v} = v/\ell$ = elastic lag displacement, Fig. 1b

$\bar{v}^g, \bar{v}^e$ = global and local approximation to $\bar{v}$

V = helicopter forward speed

$\bar{w} = w/\ell$ = elastic flap displacement, Fig. 1b

$\bar{w}^g, \bar{w}^e$ = global and local approximation to $\bar{w}$

x,y,z = rotating coordinate system, Figs. 1, $\bar{x} = x/R$

$\bar{x}_o = x_o/\ell$ = spanwise coordinate for elastic portion of the blade, Figs. 1

$\bar{x}_A = x_A/b$ = blade cross-section offset between aerodynamic and elastic centers; positive for A.C. before E.C.

$\bar{x}_I = x_I/\ell$ = blade cross-section offset between center of gravity and elastic center

x_{II} = blade cross-section offset between tension center and elastic center

$\bar{x}_e = x_e / \ell$ = element coordinate

x_L = hub loss factor

x_U = tip loss factor

$\{y\}$ = first-order state variable vector of generalized modal coordinates, Eq. (20)

$\{\bar{y}\}$ = converged nonlinear steady-state response

$\{\Delta y\}$ = perturbation of state vector about $\{\bar{y}\}$

A.1 Greek Symbols

α_R = rotor angle of attack

β_p = blade preconing, inclination of the feathering axis with respect to the hub plane, Figs. 1

γ = Lock number, $(2a\, \sigma_A\, bR^4)/I_b$

γ_F = flight path angle, measured from horizontal

$\underset{\sim}{\gamma}$ = vector of element lag interpolation polynomials

ε_D = symbolic order of magnitude quantity, equal to elastic blade slopes in bending

ζ_k = real part of λ_k

$\zeta_{iL}, \zeta_{iF}, \zeta_{iT}$ = real part of λ_k associated with predominant i-th lag, flap, or torsion mode, respectively

$\underset{\sim}{\eta}$ = vector of element flap interpolation polynomials

η_{SL}, η_{SF} = viscous structural damping coefficients in percent of critical damping for fundamental lag and flap modes, respectively

θ = collective pitch setting in hover

θ_c = critical value of θ at which linearized system is neutrally stable

θ_B = blade pretwist, built-in about elastic axis

θ_G = total geometric pitch angle, Eq. (1)

$\theta_0, \theta_{1s}, \theta_{1c}$ = collective and cyclic pitch components

λ = inflow ratio

$\lambda_0, \lambda_s, \lambda_c$ = components of λ, Eq. (2)

λ_k = k-th eigenvalue, hover; k-th characteristic exponent, forward flight

$[\Lambda]$ = modal transformation matrix, Eq. (16)

μ = advance ratio, $(V \cos \alpha_R)/(\Omega R)$

ρ_A = mass density of air

σ = solidity ratio

ϕ = elastic torsion deformation

ϕ^g, ϕ^e = global and local approximation to ϕ

$\underset{\sim}{\phi}$ = vector of element torsion interpolation polynomials

Φ_m = global shape function

$[\Phi_m]$ = matrix of global shape functions, Eq. (13)

$[\Phi(\psi)]$ = transition matrix

ψ = azimuthal angle, measured from straight aft position, dimensionless time $(\psi = \Omega t)$

$[\Psi]$ = matrix of element shape functions, Eq. (14)

ω_k = imaginary part of λ_k

$\bar{\omega}_{Ll}, \bar{\omega}_{Fl}, \bar{\omega}_{Tl}$ = first rotating uncoupled lag, flap, and torsion frequencies, respectively, nondimensionalized with respect to Ω

Ω = constant rotor speed of rotation, Figs. 1

A.2 Special Symbols

$(\dot{}) = \frac{1}{\Omega} \frac{\partial}{\partial t} = \frac{\partial}{\partial \psi}$

$( )_{,x} = \frac{\partial}{\partial \bar{x}_0}$

APPENDIX B: ELEMENT INTERPOLATION

$$\underset{\sim}{\phi} = \begin{Bmatrix} 1 - 3\bar{x}_e + 2\bar{x}_e^2 \\ 4\bar{x}_e - 4\bar{x}_e^2 \\ -\bar{x}_e + 2\bar{x}_e^2 \end{Bmatrix}$$

$$\underset{\sim}{\gamma} = \underset{\sim}{\eta} = \begin{Bmatrix} 1 - 3\dfrac{\bar{x}_e^2}{\ell_e^2} + 2\dfrac{\bar{x}_e^3}{\ell_e^3} \\ \bar{x}_e\left(1 - 2\dfrac{\bar{x}_e}{\ell_e} + \dfrac{\bar{x}_e^2}{\ell_e^2}\right) \\ 3\dfrac{\bar{x}_e^2}{\ell_e^2} - 2\dfrac{\bar{x}_e^3}{\ell_e^3} \\ \bar{x}_e\left(-\dfrac{\bar{x}_e}{\ell_e} + \dfrac{\bar{x}_e^2}{\ell_e^2}\right) \end{Bmatrix}$$

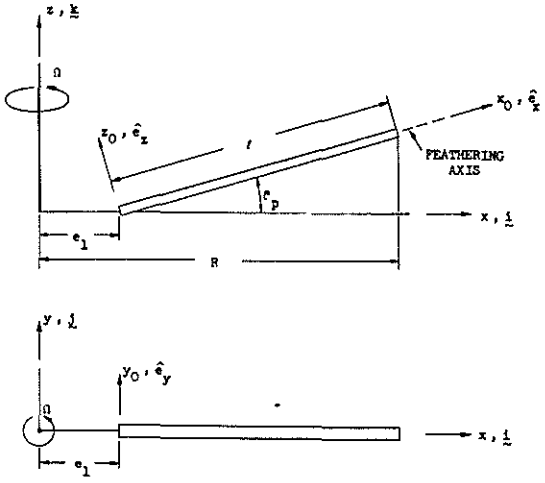

Fig. 1a Typical Description of the Undeformed Blade in the Rotating System x,y,z ($\underset{\sim}{i}$, $\underset{\sim}{j}$, $\underset{\sim}{k}$)

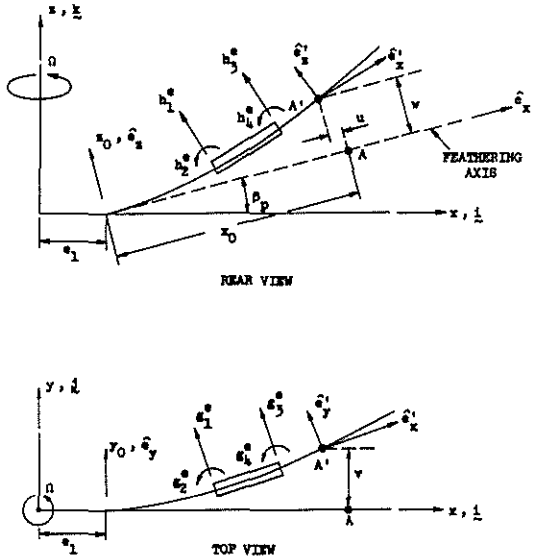

Fig. 1b Geometry of the Elastic Axis of the Deformed Blade and Schematic Description of the Finite Element Model for Flap and Lag

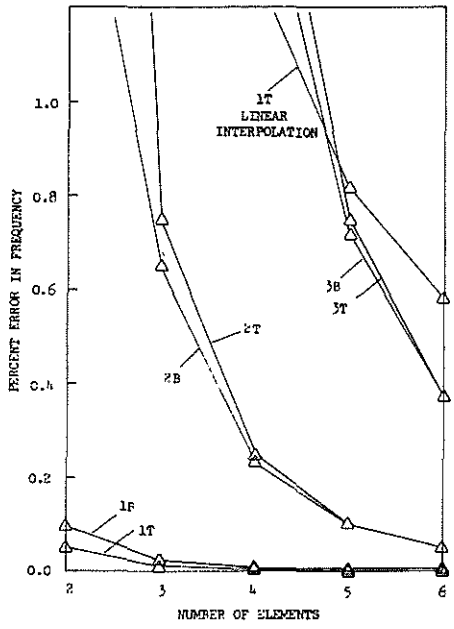

Fig. 2 Accuracy of the First, Second and Third Bending and Torsion Frequency Versus Number of Elements for a Nonrotating Uniform Beam

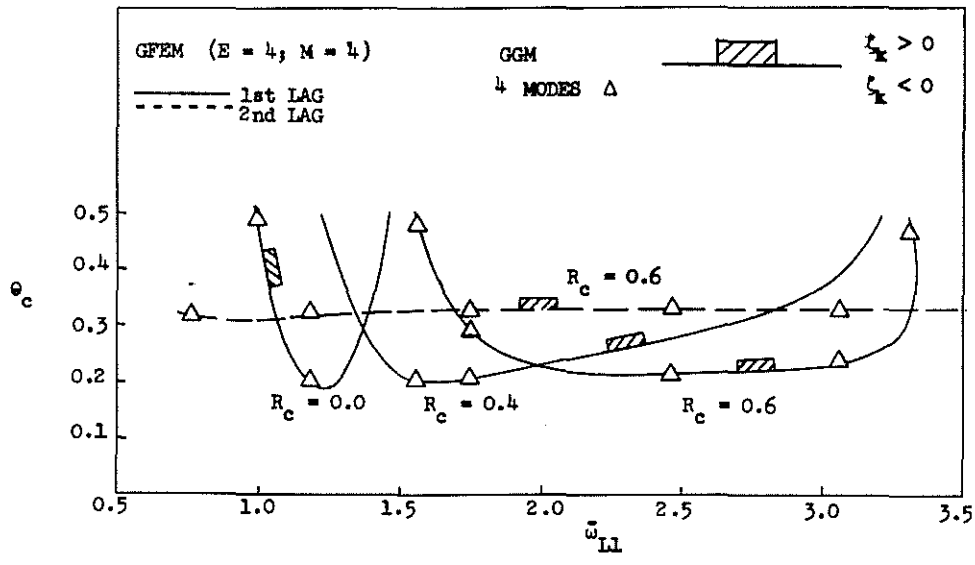

Fig. 3 Comparison of Flap-Lag Stability Boundaries When Using GFEM Versus Global Galerkin Method (GGM)
(σ = 0.10; γ = 5.0; $\bar{\omega}_{F1}$ = 1.15; $\bar{b}$ = .0313)

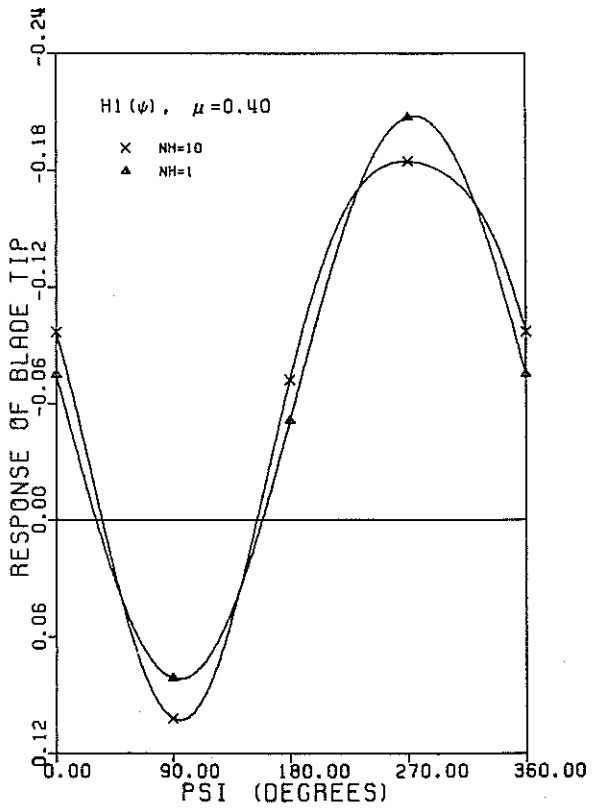

Fig. 4 Contribution of Higher Harmonics to the Lag Steady-State Response ($N_{psi} = N_{rki} = 120$; k = 1)

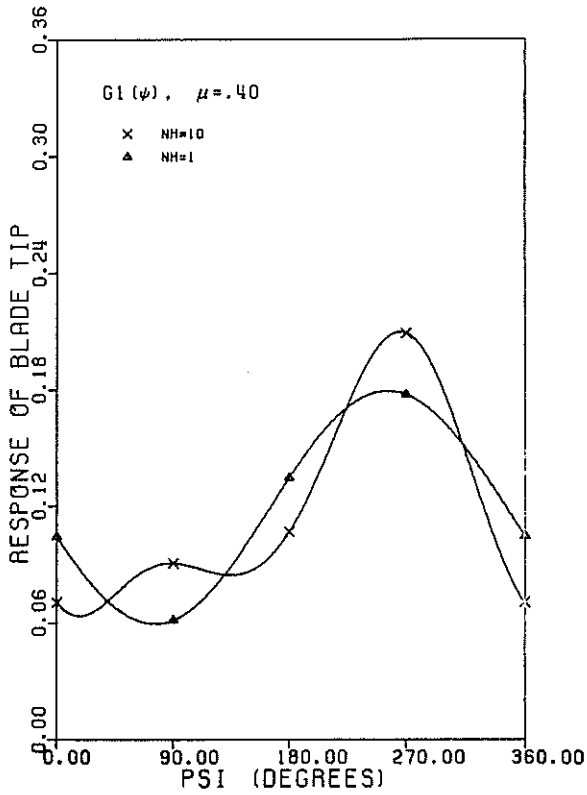

Fig. 5 Contribution of Higher Harmonics to the Flap Steady-State Response ($N_{psi} = N_{rki} = 120$; k = 1)

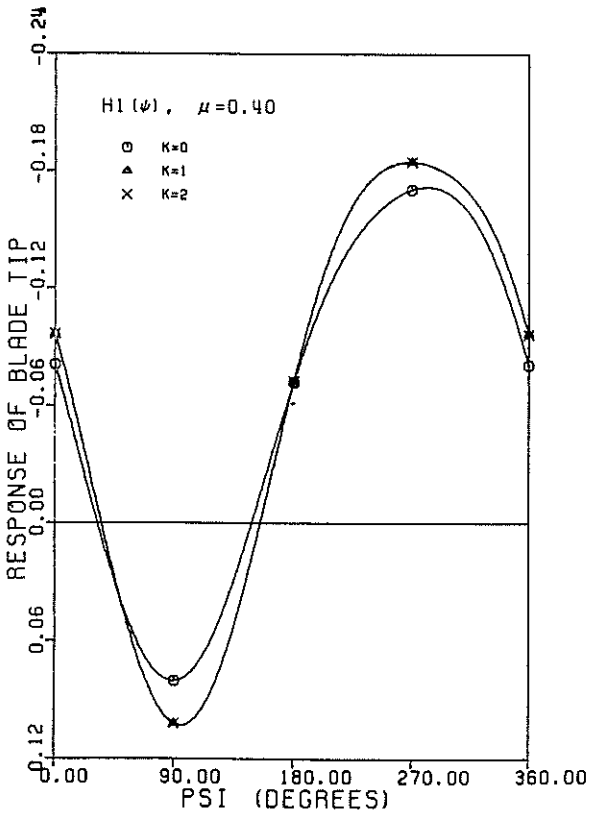

Fig. 6 Effect of Nonlinear Terms on Lag Steady-State Response ($N_{psi} = N_{rki} = 120$)

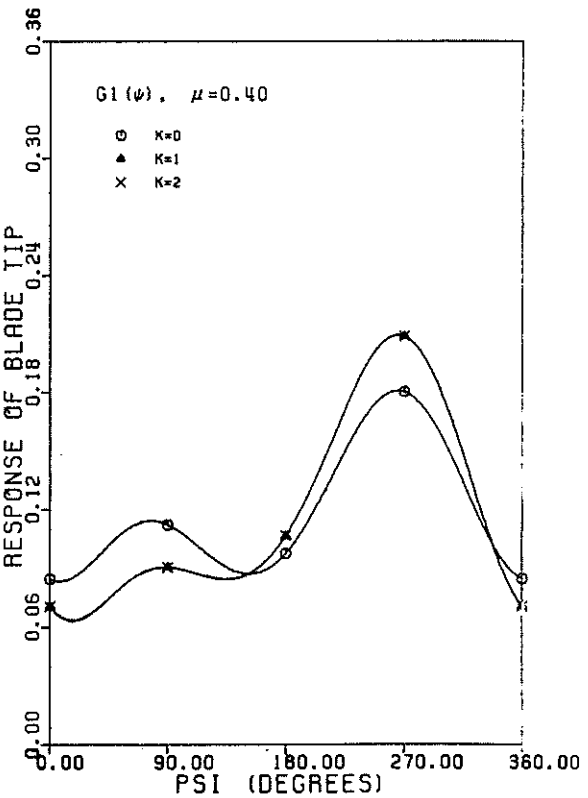

Fig. 7 Effect of Nonlinear Terms on Flap Steady-State Response ($N_{psi} = N_{rki} = 120$)

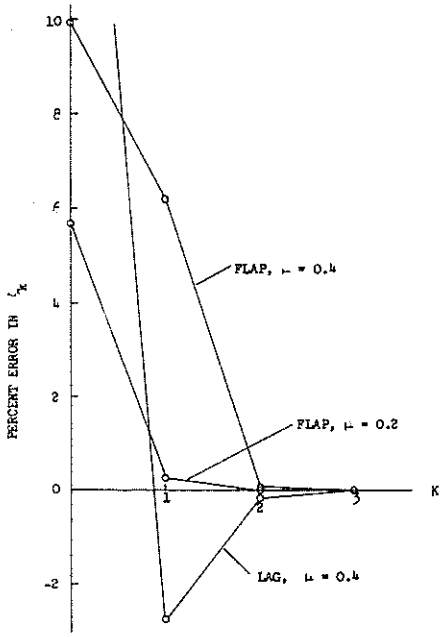

Fig. 8 Convergence of Real Parts of Characteristic Exponents as a Function of the Number of Quasi-linearization Steps ($N_{psi} = N_{rki} = 120$)

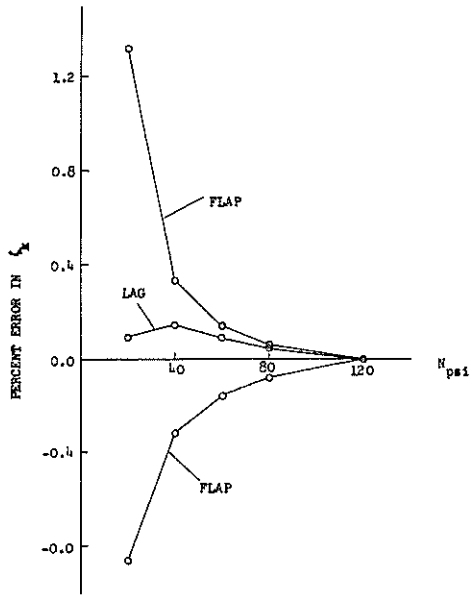

Fig. 9 Convergence of Real Parts of Characteristic Exponents as a Function of the Number of Azimuthal Steps ($N_{psi} = N_{rki}$; k = 3)

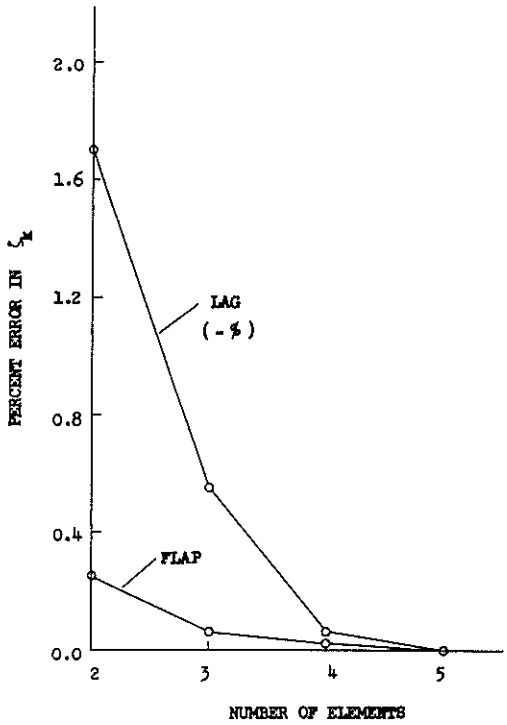

Fig. 10 Convergence of Flap-Lag Stability When the Number of Elements is Changed ($M = 2$; $\bar{\omega}_{Ll} = 0.732$; $R_c = 0.6$; $\mu = 0.4$)

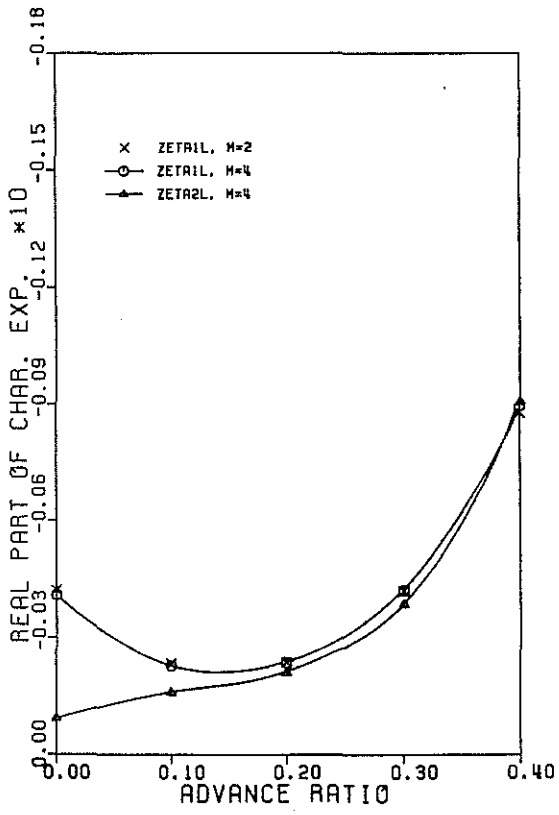

Fig. 11 Lag Stability When the Number of Modes is Changed
($E = 4$; $\bar{\omega}_{L1} = 0.732$; $R_c = 0.6$)

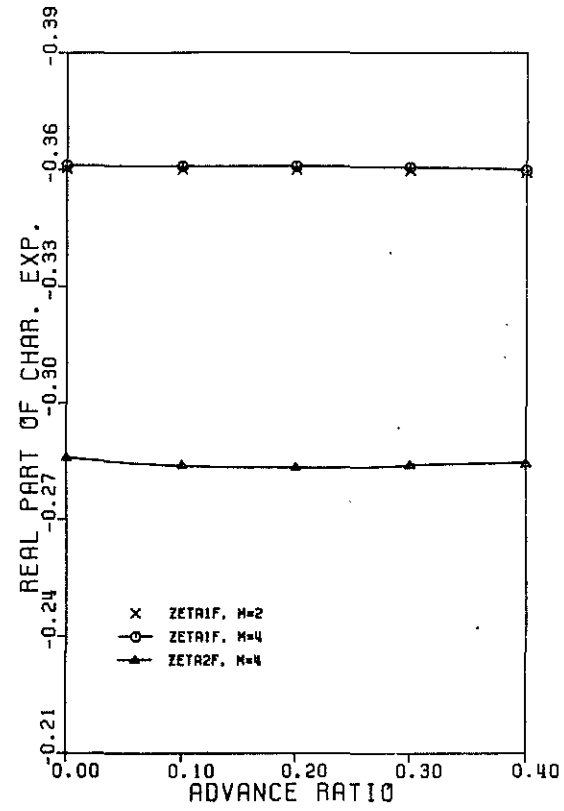

Fig. 12 Flap Stability When the Number of Modes is Changed
($E = 4$; $\bar{\omega}_{L1} = 0.732$; $R_c = 0.6$)

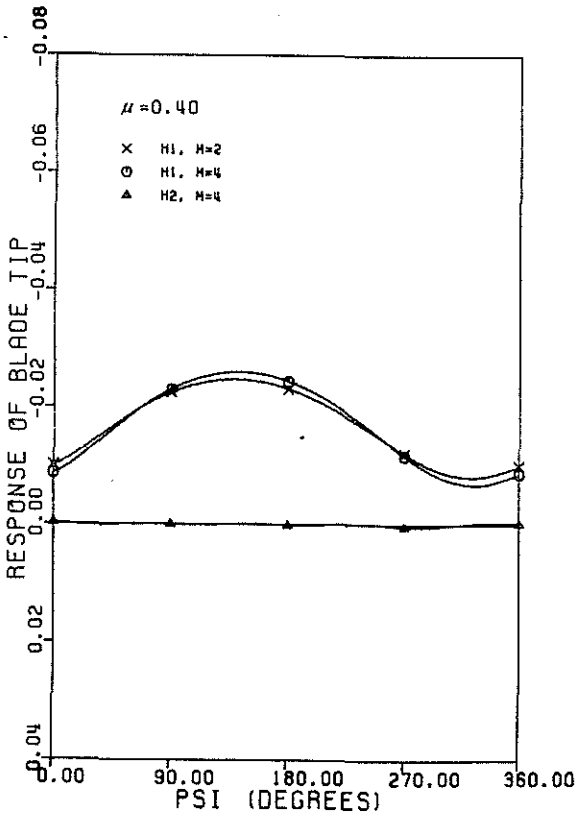

Fig. 13 Lag Steady-State Response When the Number of Modes is Changed
($E = 4$; $\bar{\omega}_{L1} = 0.732$; $R_c = 0.6$)

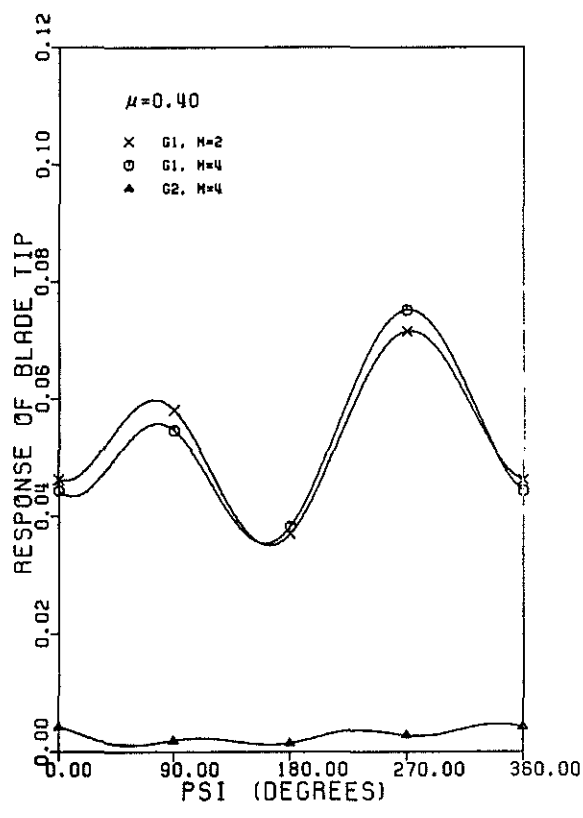

Fig. 14 Flap Steady-State Response When the Number of Modes is Changed
($E = 4$; $\bar{\omega}_{L1} = 0.732$; $R_c = 0.6$)

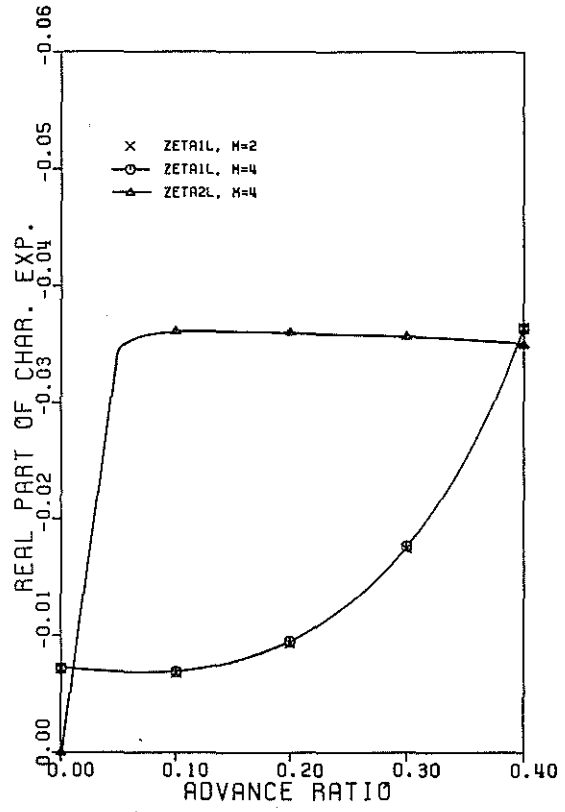

Fig. 15 Lag Stability When the Number of Modes is Changed, Stiff Inplane Blade ($E = 4$; $\bar{\omega}_{L1} = 1.417$; $R_c = 0.8$; $C_W = .01$)

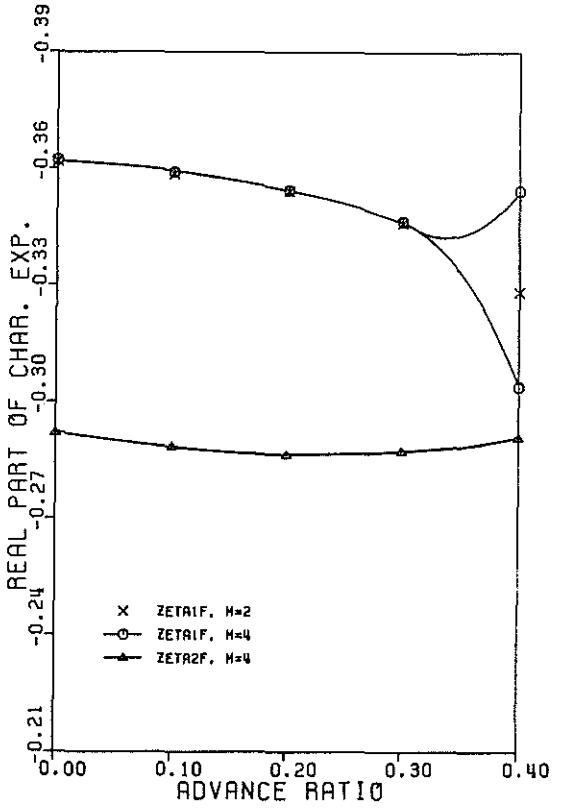

Fig. 16 Flap Stability When the Number of Modes is Changed, Stiff Inplane Blade ($E = 4$; $\bar{\omega}_{L1} = 1.417$; $R_c = 0.8$; $C_W = .01$)

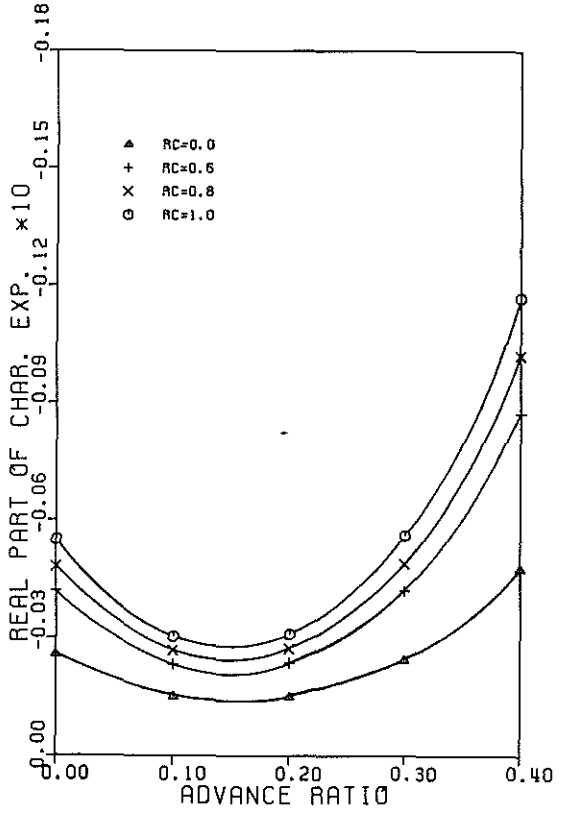

Fig. 17 Effect of Elastic Coupling on First Lag Mode Stability ($E = 3$; $M = 2$; $\bar{\omega}_{L1} = 0.732$)

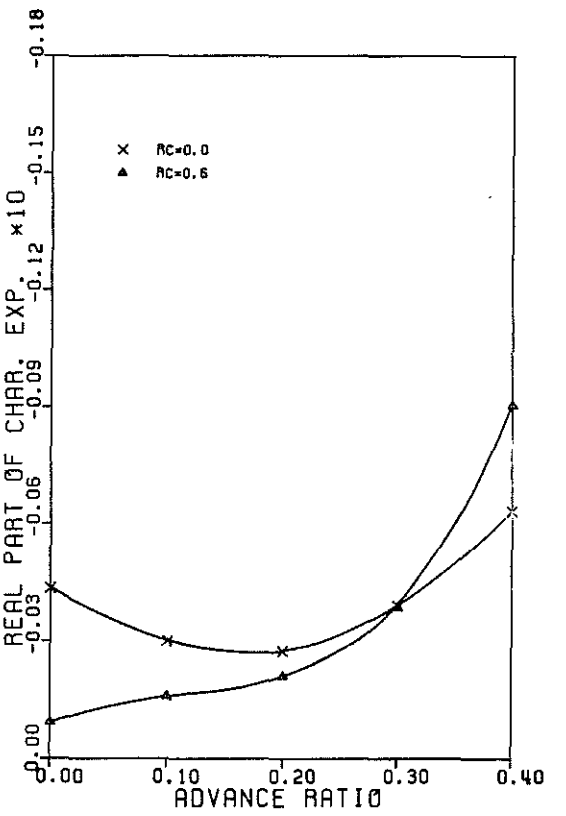

Fig. 18 Effect of Elastic Coupling on Second Lag Mode Stability ($E = 4$; $M = 4$; $\bar{\omega}_{L1} = 0.732$)